

Single-Molecule Vibrational Spectroscopy of H₂O on Anatase TiO₂ (101)

Christian Dette[†], Miguel A. Perez-Osorio[‡], Shai Mangel[†], Feliciano Giustino[‡], Soon Jung Jung^{†,*}, and Klaus Kern^{†,§}

[†]Max Planck Institute for Solid State Research, Heisenbergstrasse 1, 70569 Stuttgart (Germany).

[‡]Department of Materials, University of Oxford, Parks Road, Oxford OX1 3PH (United Kingdom).

[§]Institut de Physique, École Polytechnique Fédérale de Lausanne, 1015 Lausanne (Switzerland).

Supporting Information Placeholder

ABSTRACT: Atomic level understanding of water on titanium dioxide (TiO₂), in particular the mineral form anatase, is exceptionally important, considering its practical applications including photocatalytic water-splitting, photo-induced hydrophilicity and water purification.¹⁻³ Although much effort has been devoted to the study of water adsorption on anatase, the lack of chemical identification on the single molecular level still hinders fundamental research, such as investigating the elemental steps of water splitting. Here, we have unequivocally identified single water molecules and hydroxyls on the TiO₂ anatase (101) surface using scanning tunneling microscopy (STM) in combination with inelastic tunneling spectroscopy (IETS). Single molecule labelling on the semiconductor surface was confirmed by demonstrating the isotope shift of the vibrational signatures and by first-principles density functional theory (DFT). The chemical identification of individual water molecules on anatase opens a new path towards a better understanding of water splitting processes.

Substantial effort has been devoted to understand the interaction of H₂O with TiO₂ using an arsenal of spectroscopic tools such as photoelectron spectroscopy (PES), infrared spectroscopy (IRS) and temperature programmed desorption (TPD) in conjunction with DFT calculations.⁴⁻⁷ In particular, the physical and chemical properties of oxygen vacancies and their effect on surface reactions have been intensively studied.⁴ In general, these spectroscopic techniques detect and average signal obtained over large area ($\geq 100 \times 100 \text{ nm}^2$). To understand the elementary steps of water splitting, particularly the role of photogenerated holes and electrons, the direct probing of adsorbed species at the atomic scale is essential, for which STM has been proven to be an ideal tool. However, the key components of water splitting, H₂O and OH, appear too similar in STM topography to distinguish the individual species.^{8,9} Although the behavior of H₂O and OH in electric fields were used as a tentative assignment,⁹ no clear chemical identification was given so far. This ambiguity has generated significant controversy^{9,10} and remains one of the greatest obstacles to microscopic understanding of water splitting on anatase. Even simple questions, such as ‘Can water thermally dissociate at room temperature?’ could not be answered in an unequivocal way.^{9,11,12} Although there are experimental results which prove a dissociative adsorption of water at high coverage,^{12,13} none could prove the occurrence of thermally dissociated single water molecules. The behavior of isolated water is inherently different to multilayer water in which intermolecular hydrogen bond-

ing can stabilize dissociated water. Here, we address this challenge by using molecular vibrations obtained in STM-IETS as fingerprints to label individual molecules with high chemical sensitivity. In STM-IETS, the tip is fixed at a position over the surface and the bias voltage is swept to record an I-V curve. Once the applied bias voltage exceeds the energy of a molecular vibration, an additional tunnel channel opens increasing the conductance of the tip-sample junction. This is recorded as a peak in the d^2I/dV^2 spectrum. This technique was first demonstrated in a pioneering experiment with single acetylene molecules on the Cu(100) surface¹⁴ and since then has been very successfully applied to explore single molecule chemistry on metal surfaces.¹⁵

However, for semiconductors recording of STM-IETS is challenging due to the absence of states around the Fermi level (E_F). To our knowledge no successful experiment has been reported thus far. However, by using a highly *n*-doped naturally grown TiO₂ anatase (101) crystal, we demonstrate in the present letter that we have a finite Fermi surface, which allows detecting vibrational modes of molecular and dissociated water on the anatase surface. These findings could potentially be transferred to any molecular/semiconductor system, if one can provide enough states around E_F of the semiconductor.

Figure 1a shows an empty-state STM topograph of a TiO₂ anatase (101) surface after deposition of H₂O molecules (detailed procedure in Methods). The sample was maintained at 120 K during vapor deposition to allow molecular adsorption.⁵ This preparation leads to the formation of thin ice covering the anatase surface (Supplementary Figure S2). In a second step the sample was heated to room temperature resulting in single random molecular adsorption as shown in Figure 1a. These conditions favor random molecular distribution with only a limited number of aggregates observed on terraces or step edges. The adsorbed molecules appear in a dumbbell shape of 0.9 nm in length. These protrusions are above the Ti-O dimer row with their centers on top of a surface Ti_{sc} atom. The STM features can be differentiated further, as highlighted in high resolution STM topographic images showing two individual molecules (Figs. 1b and d). The same images are represented in a different color code to facilitate distinguishing both species in Figures 1c and e. Whereas the top molecule (red squared) has a symmetric dumbbell shape, the lower molecule (green squared) is slightly asymmetric in size. The population of symmetric and asymmetric protrusions in several selected areas were manually counted and a ratio of approximately 7 to 3 was obtained (cf. Supplementary Figure S6).

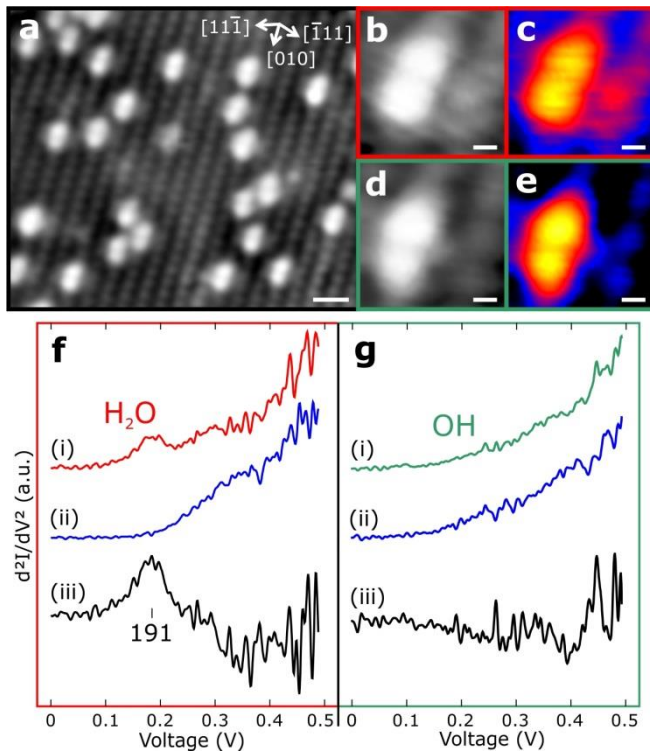


Figure 1. H_2O and OH adsorption on TiO_2 anatase (101). (a) Empty-state STM image shows water adsorption on atomically resolved TiO_2 ($V_s = 1 \text{ V}$, $I = 1 \text{ nA}$, $T = 5 \text{ K}$). (b-e) High-resolution STM images (linear scale) showing two isolated molecules of 1.4 \AA in height with different features – a symmetric (red squared, b and c) and an asymmetric (green squared, d and e)). f, IETS spectra ($V_s = 0.5 \text{ V}$, $I = 0.1 \text{ nA}$) taken on the symmetric protrusion from (b) (i), pristine anatase (ii), and the difference spectrum (iii) show a distinct feature at 191 mV , which can be assigned to the $\delta(\text{H-O-H})$ bending mode, and broad peaks in between $300\text{-}500 \text{ mV}$ ($\nu(\text{O-H})$ stretching modes). The chemical fingerprint identifies the symmetric protrusion to be a H_2O molecule. (g) In the case of the asymmetric protrusion (c) the bending mode is missing but the stretching modes are present ($400\text{-}500 \text{ mV}$) allowing us to label it as a dissociated water (OH). (scalebars: (a) = 1 nm ; (b) – (e) = 0.2 nm)

In order to identify these two species, IETS was performed. Owing to the importance of the tip apex to the STM-IETS measurement and the frequent changes that can occur even during a measurement,¹⁶ we obtained the substrate spectra immediately prior and following to the spectra measured on the molecule. Figure 1f shows the IETS data obtained on the symmetric molecule from Figure 1b (i), on the pristine TiO_2 anatase (101) surface (ii), and the corresponding difference spectrum (iii). As shown in the spectra of pristine TiO_2 anatase (101), the density of states increases strongly for high bias voltages ((ii) in Figure 1). This leads to a higher level of noise limiting the resolution of IETS peaks in the range. The data reveal a clear peak around 191 mV which can be assigned to the molecular $\delta(\text{H-O-H})$ bending mode.^{17,18} The broad and complex feature in the region between $300 - 500 \text{ mV}$, with a maximum around 470 mV , arises from the superposition of various symmetric and antisymmetric $\nu(\text{O-H})$ stretch modes.^{18,19} Due to the increased noise level that is present at higher voltages and the complex-

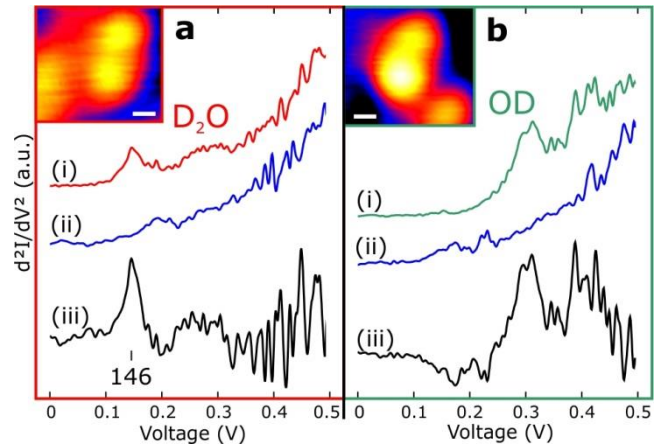


Figure 2. D_2O and OD adsorption on TiO_2 anatase (101). (a) IETS spectra obtained on D_2O with a neighboring water molecule (insert: STM image, i), pristine anatase (ii), and the difference spectrum (iii) reveal a distinct feature at 146 mV associated to the $\delta(\text{D-O-D})$ bending mode and multiple features around 300 mV which can be attributed to symmetric and asymmetric stretch modes. (b) IETS spectra obtained on OD with a neighboring molecule (insert: OD molecule) showing the stretch mode around 300 mV but no feature around 150 mV . (scalebars: inserts in (a),(b) = 0.2 nm)

ity of the stretch modes, it is very difficult to distinguish each component involved in the $\nu(\text{O-H})$ stretch modes. However, the clear feature of the bending mode and the range of the stretch modes, which fit well with previous reports, are enough to identify the individual protrusions. The green spectrum in Figure 1g is recorded on the asymmetric molecule showing only broad peaks at higher energies around 480 mV , but no features around 200 mV . These findings allow us to label the symmetric protrusion (red, 1b) a H_2O molecule while the asymmetric protrusion (green, 1d) is a hydroxyl species (OH) resulting from water dissociation (further discussed below).

To confirm the origin of the vibrational peaks, hydrogen was substituted by deuterium and the isotopic shifts of the molecular fingerprints were studied.¹⁹ For this, the TiO_2 anatase (101) crystal was cleaned and subsequently D_2O was adsorbed. Due to the similarity in the adsorption energies indicated by TPD data,⁵ our preparation process for deuterated water was the same as for H_2O . The protrusions in the STM topographs have a similar size as in the case of the H_2O molecules (0.9 nm) and appear again as symmetric or asymmetric dumbbell shapes. IETS measurements shown in Figure 2a on a symmetric molecule with a neighbor (red-squared) reveal a sharp feature at 146 mV and broader peaks in the region around 300 mV . Since the replacement of hydrogen by deuterium induces a redshift of the vibrational peaks, we can again assign the lower energy feature to the $\delta(\text{D-O-D})$ bending mode. The redshift factor is approximately $3/4$ and in good agreement with previous results proving the origin of the inelastic features to be vibrational excitations.¹⁹ IETS measurements on the asymmetric molecule reveal a similar vibrational energy for the $\nu(\text{O-D})$ stretch mode (around 300 mV) and again no feature in the energy range of the bending mode. Therefore, the symmetric molecule is a molecular D_2O (a) while the asymmetric molecule is a hydroxyl OD (b).

Based on our topographic and spectroscopic data, the expected adsorption structure of H_2O and dissociated water ($\text{OH}+\text{H}$) was calculated. Figures 3a and c show the corresponding results in the presence

of an electric field generated by the STM tip (see SI for further details about the electric field effect). The oxygen of the H_2O molecule forms a dative bond to a surface Ti_{sc} whereas the oxygen of the OH forms a covalent bond (Figure 3a). Under given electric field, both H_2O and OH molecules are aligned perpendicular to the surface, with the H atoms pointing upward. The corresponding STM images are presented in Figures 3b and d. Both protrusions are positioned on top of the Ti-O dimers centering on surface Ti_{sc} atoms. The calculated STM images reproduce the symmetry of molecular water and the asymmetry of dissociated water molecules observed in the experiment. Given the low diffusion barrier of hydrogen we calculated STM images for hydroxyls with and without hydrogen in the vicinity; the calculated STM images of OH were not affected by the position of adjacent H.

The vibrational frequencies and infrared intensities were calculated using density functional perturbation theory (DFPT). We present the vibrational frequencies of the ground state, since the frequency shift induced by an applied electric field was negligible in given condition. For a single molecular H_2O , the calculated frequency of the $\delta(\text{H-O-H})$ bending mode is 195 meV, and the calculated frequency of the symmetric and asymmetric $\nu(\text{O-H})$ stretching modes are 459 and 472 meV, respectively. In the case of the hydroxyl group, the $\nu(\text{O-H})$ stretching mode is calculated to be 472 meV. These values are in good agreement with the experimental data. Furthermore, we calculated the effect of hydrogen bonding to a neighboring water molecule, which frequently occurs (Figure 2). In FTIR, monolayer to multilayer coverages of water are measured and hence, water always forms hydrogen bonds with neighboring molecules. The influence on the stretch modes is discussed in the supplemental information.

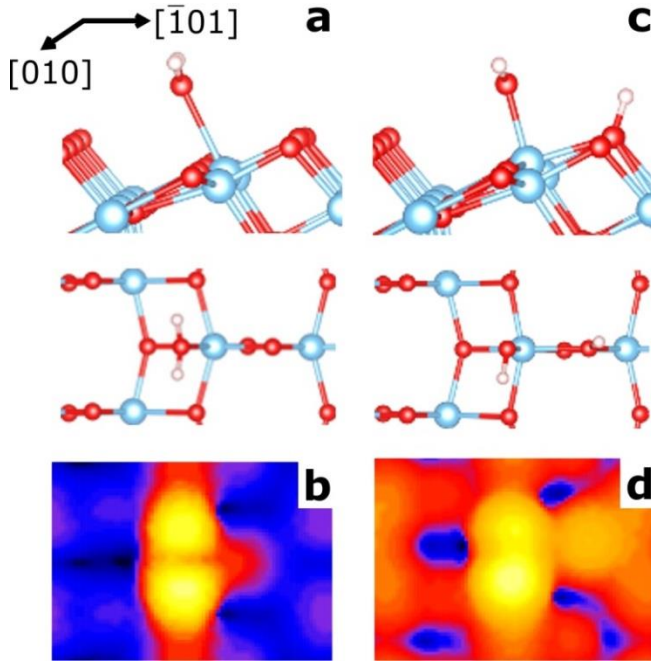


Figure 3. Ball-and-stick models and calculated STM images of molecular and dissociated water on TiO_2 . (a),(c) Atomistic model of the H_2O molecule and dissociated water ($\text{OH} + \text{H}$) in presence of an applied electric field. (b),(d) their corresponding calculated STM images. The STM images were calculated at constant current by considering the electronic states within 0.7 eV from the conduction band edge. The magnitude of the applied electric field was 5×10^9 V/m corresponding to a tip bias voltage of 1-3 V.

Units: meV	DFT	STM-IETS	ATR-FTIR ¹⁸
Single H_2O	195	191	
H_2O complex	199	201	203
Single D_2O	143	146	
D_2O complex	146	147	149

Table 1. Comparison of theoretical and experimental bending mode energies.

As shown in Figure 1, around 30 % of the observed protrusions appear asymmetric which can be assigned to hydroxyls resulting from water dissociation (Supplementary Figure S6). Since there was no illumination during our preparation procedure, we exclude photo-induced dissociation. Hence, we consider the possibility of thermal dissociation by calculating the energy diagram of water dissociation reaction (as shown in Figure 4). The first step of water dissociation is

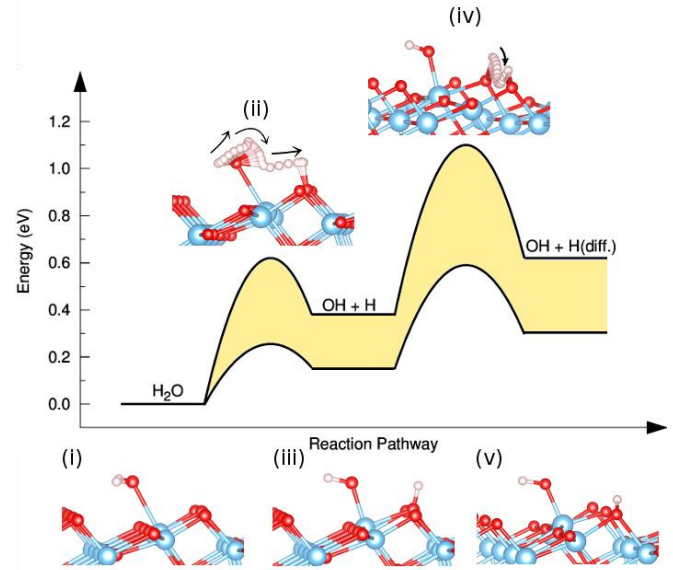


Figure 4. Calculated dissociation barrier for water on TiO_2 anatase (101) surface and diffusion barrier for H proton on the surface, and ball-and-stick models of the H_2O molecule, hydroxyl group and the intermediate activate complexes. Upper curve: reaction pathway calculated with a slab containing 4 TiO_2 layers, and by sampling the first Brillouin zone at the Gamma point. Lower curve: reaction pathway estimated from calculations of the dissociation energies between the configurations (i), (iii), and (v), using a larger slab (8 layers) and a finer ($2 \times 2 \times 1$) sampling of the Brillouin zone. In the lower curve the reaction barriers were estimated by scaling the barriers calculated in the upper curve via the ratios of the corresponding dissociation energies. The dissociation of (i) the H_2O molecule to (iii) $\text{OH} + \text{H}$ occurs via (ii) an intermediate activated complex, for which we estimated an activation energy $E_a = 0.26$ eV. This reaction is endothermic with an enthalpy $\Delta H = +0.67$ eV. The subsequent diffusion of the H proton on the surface, from (iii) to (v), can take place by overcoming a potential barrier for which we estimate an activation energy $E_a = 0.44$ eV. The diffusion reaction is also endothermic with an enthalpy $\Delta H + 0.75$ eV. The dissociation and diffusion barriers in the upper curve were calculated using the nudged elastic band method (NEB) at the DFT+U level, with a Hubbard parameter of 3.5 eV (see Methods for further details and videos S3 and S4 in SI, which corresponds to our NEB calculations of water dissociation and H proton diffusion).

formation of an intermediate complex (Figure 4(ii)), for which one hydrogen bond of the water molecule is weakened due to interaction with a neighboring surface O_{2c} . Then, this hydrogen separates from the water molecule to create a $H-O-Ti_{5c}$ and $H-O_{2c}$ complex (Figure 4(iii)). The activation energy of the intermediate complex is around 0.26 eV. The dissociated state is energetically less favorable by 0.16 eV compared to the molecular water, suggesting the reaction to be endothermic. Owing to the relatively low height of the calculated dissociation barrier, the thermal dissociation of water at room temperature is highly favored. The subsequent diffusion of the H proton to the nearest-neighbor O_{2c} atom has an activation energy of 0.44 eV, which is low enough to occur at room temperature. Nevertheless, these theoretical results should be taken as a qualitative description because, as already pointed out in Ref. ¹³, we found that the energetics of the molecular and dissociated water is sensitive to parameters used in the calculations. For example, using a larger slab and a finer sampling of the Brillouin zone, the calculated energy is apparently reduced (Figure 4).

Once we consider only the calculated energy value, the 30 % of dissociated water cannot be present. However, enthalpy is a state function, which means the value is only dependent on the initial and final enthalpies. Noticing the low diffusion barrier of the dissociated hydrogen atom on the anatase surface which blocks the reverse reaction, the expected population of OH should be increased. In addition, the dissociated state becomes more stable than the water molecule when the molecules are positioned close enough to the adjacent molecules enabling the hydrogen bonding.¹³ Therefore, we conclude that the hydroxyl group which appeared as asymmetric protrusion is thermally dissociated water. Moreover, we have performed experiments where the sample was never heated above 77 K. This preparation method only led to the adsorption of non-dissociated water molecules (manuscript in preparation).

In this study, STM-IETS was employed to obtain clear chemical identification and structural analysis of molecules on the semiconductor surface. The combination of STM-IETS and theoretical analyses succeeded to distinguish water molecules and hydroxyls on the TiO_2 anatase (101) substrate using vibrational fingerprints. We showed that water dissociates thermally at room temperature. The identification of these individual species enables further studies on the fundamental processes of photocatalytic water splitting, including active sites on the anatase surface, the role of photogenerated charge carriers, and the details of charge transfer processes.

ASSOCIATED CONTENT

Supporting Information

Experimental Section, Influence of Hydrogen Bonding to the Vibration Modes, Calculation of the Electric Field Effect

AUTHOR INFORMATION

Corresponding Author

*s.jung@fkf.mpg.de

Notes

The authors declare no competing financial interests.

ACKNOWLEDGMENT

M.A.P.O. and F.G. gratefully acknowledge funding from the Leverhulme Trust (Grant RL-2012-001), the UK Engineering and Physical Sciences Research Council (grants No. EP/J009857/1 and EP/M020517/1), and the Graphene Flagship (EU FP7 grant no. 604391), and supercomputing time at the University of Oxford Advanced Research Computing (ARC) facility (<http://dx.doi.org/10.5281/zenodo.22558>), the ARCHER UK National Supercomputing Service under the 'AMSEC' Leadership project and the 'CTOA' RAP project, and the Cartesius Dutch National Supercomputer under the PRACE DECI-13 project.

REFERENCES

- (1) Fujishima, A.; Honda, K. *Nature* **1972**, *238*, 37.
- (2) Wang, R.; Hashimoto, K.; Fujishima, A.; Chikuni, M.; Kojima, E.; Kitamura, A.; Shimohigoshi, M.; Watanabe, T. *Nature* **1997**, *388*, 431.
- (3) Mills, A.; Davies, R. H.; Worsley, D. *Chem. Soc. Rev.* **1993**, *22*, 417.
- (4) Oviedo, J.; Sánchez-de-Armas, R.; San Miguel, M. Á.; Sanz, J. F. *J. Phys. Chem. C* **2008**, *112*, 17737.
- (5) Herman, G. S.; Dohnálek, Z.; Ruzycki, N.; Diebold, U. *J. Phys. Chem. B* **2003**, *107*, 2788.
- (6) Kurtz, R. L.; Stock-Bauer, R.; Msdey, T. E.; Román, E.; De Segovia, J. L. *Surf. Sci.* **1989**, *218*, 178.
- (7) Primet, M.; Pichat, P.; Mathieu, M. V. *J. Phys. Chem.* **1971**, *75*, 1216.
- (8) Stetsovych, O.; Todorovic, M.; Shimizu, T. K.; Moreno, C.; Ryan, J. W.; Leon, C. P.; Sagisaka, K.; Palomares, E.; Matolin, V.; Fujita, D.; Perez, R.; Custance, O. *Nat Commun* **2015**, *6*.
- (9) Setvin, M.; Daniel, B.; Aschauer, U.; Hou, W.; Li, Y.-F.; Schmid, M.; Selloni, A.; Diebold, U. *PCCP* **2014**, *16*, 21524.
- (10) Setvin, M.; Aschauer, U.; Scheiber, P.; Li, Y.-F.; Hou, W.; Schmid, M.; Selloni, A.; Diebold, U. *Science* **2015**, *349*, aac9659.
- (11) He, Y.; Tilocca, A.; Dulub, O.; Selloni, A.; Diebold, U. *Nat Mater* **2009**, *8*, 585.
- (12) Walle, L. E.; Borg, A.; Johansson, E. M. J.; Plogmaker, S.; Rensmo, H.; Uvdal, P.; Sandell, A. *J. Phys. Chem. C* **2011**, *115*, 9545.
- (13) Patrick, C. E.; Giustino, F. *Phys. Rev. Applied* **2014**, *2*, 014001.
- (14) Stipe, B. C.; Rezaei, M. A.; Ho, W. *Science* **1998**, *280*, 1732.
- (15) Chiang, C.-I.; Xu, C.; Han, Z.; Ho, W. *Science* **2014**, *344*, 885.
- (16) Wahl, P.; Diekhöner, L.; Schneider, M. A.; Kern, K. *Rev. Sci. Instrum.* **2008**, *79*, 043104.
- (17) Maira, A. J.; Coronado, J. M.; Augugliaro, V.; Yeung, K. L.; Conesa, J. C.; Soria, J. *J. Catal.* **2001**, *202*, 413.
- (18) Belhadj, H.; Hakki, A.; Robertson, P. K. J.; Bahnemann, D. W. *PCCP* **2015**, *17*, 22940.
- (19) Nakamoto, K. In *Handbook of Vibrational Spectroscopy*; John Wiley & Sons, Ltd: **2006**.

